# A self-powered ultraviolet photodetector based on a $Ga_2O_3/Bi_2WO_6$ heterojunction with low noise and stable photoresponse

Li-Li Yang(杨莉莉)[1,2], Yu-Si Peng(彭宇思)[3], Zeng Liu(刘增)[1,2], Mao-Lin Zhang(张茂林)[1,2], Yu-Feng Guo(郭宇锋)[1,2], Yong Yang(杨勇)[3], and Wei-Hua Tang(唐为华)[1,2,†]

[1] *College of Integrated Circuit Science and Engineering, Nanjing University of Posts and Telecommunications, Nanjing* 210023, *China*
[2] *National and Local Joint Engineering Laboratory for RF Integration and Micro-Packing Technologies, Nanjing University of Posts and Telecommunications, Nanjing* 210023, *China*
[3] *State Key Laboratory of High Performance Ceramics and Superfine Microstructures, Shanghai Institute of Ceramics, Chinese Academy of Sciences, Shanghai* 200050, *China*

(Received 31 March 2022; revised manuscript received 10 June 2022; accepted manuscript online 14 June 2022)

A self-powered solar-blind ultraviolet (UV) photodetector (PD) was successfully constructed on a $Ga_2O_3/Bi_2WO_6$ heterojunction, which was fabricated by spin-coating the hydrothermally grown $Bi_2WO_6$ onto MOCVD-grown $Ga_2O_3$ film. The results show that a typical type-I heterojunction is formed at the interface of the $Ga_2O_3$ film and clustered $Bi_2WO_6$, which demonstrates a distinct photovoltaic effect with an open-circuit voltage of 0.18 V under the irradiation of 254 nm UV light. Moreover, the $Ga_2O_3/Bi_2WO_6$ PD displays excellent photodetection performance with an ultra-low dark current of $\sim 6$ fA, and a high light-to-dark current ratio (PDCR) of $3.5 \times 10^4$ in self-powered mode (0 V), as well as a best responsivity result of 2.21 mA/W in power supply mode (5 V). Furthermore, the PD possesses a stable and fast response speed under different light intensities and voltages. At zero voltage, the PD exhibits a fast rise time of 132 ms and 162 ms, as well as a quick decay time of 69 ms and 522 ms, respectively. In general, the newly attempted $Ga_2O_3/Bi_2WO_6$ heterojunction may become a potential candidate for the realization of self-powered and high-performance UV photodetectors.

**Keywords:** $Ga_2O_3/Bi_2WO_6$ heterojunction, UV photodetector, self-powered operation

**PACS:** 73.40.–c, 73.40.Lq, 73.50.Pz **DOI:** 10.1088/1674-1056/ac7865

## 1. Introduction

Due to the advantages of non-line-of-sight communication, high security and strong anti-interference capabilities, solar-blind deep ultraviolet (UV) detection technology operating in a wavelength shorter than 280 nm exhibits broad application prospects in both military and civilian fields, including national defense warning and tracking, flame alarm, ozone hole monitoring, etc.[1,2] Solar-blind deep UV detectors work mainly based on the photovoltaic effect of semiconductors with wide band gaps over 4.4 eV. Although $Al_xGa_{1-x}N$, $Zn_xMg_{1-x}O$ and diamond all have wide band gaps, $Al_xGa_{1-x}N$ is prone to high-density defects when a high Al content of 40% is necessary. Meanwhile, $Zn_xMg_{1-x}O$ tends to undergo phase separation when the relative content of Mg meets the requirement for a wider band gap, and diamond only responds to light with wavelengths shorter than 225 nm.[3,4] Gallium oxide ($Ga_2O_3$) has five different phases ($\alpha$, $\beta$, $\gamma$, $\varepsilon$, and $\delta$), which endow it with an adjustable band gap in the range of 4.5 eV–5.3 eV,[5–9] precisely corresponding to the response light wavelength range below 280 nm. Among them, the monoclinic $Ga_2O_3$ ($\beta$-$Ga_2O_3$) is the most thermodynamically stable phase, with an intrinsic band gap of about 4.8 eV, good mobility (100 $cm^2/(V{\cdot}s)$) and a high breakdown field (8 MV/cm).[10–12] Furthermore, the high-quality $\beta$-$Ga_2O_3$ films can be successfully prepared by various techniques,[13,14] such as metal organic chemical vapor deposition (MOCVD), molecular beam epitaxy (MBE) and halide vapor phase epitaxy (HVPE), which promote $Ga_2O_3$ as one of the most suitable candidates for solar-blind UV detectors.

According to the device structure, $Ga_2O_3$-based solar-blind UV detectors mainly include metal–semiconductor–metal (MSM), heterojunction and Schottky photodiode detectors. Among them, the $Ga_2O_3$-based heterostructure photodetector (PD) exhibits many excellent properties, including low dark current, strong sensitivity, high photoresponsivity, as well as a self-powered supply by constructing the interfacial depletion region between two different semiconductor materials. It thus receives a lot of attention from researchers. Many materials have been reported to form heterojunctions with $Ga_2O_3$, such as graphene, $Ti_3C_2$, $BiFeO_3$, $CsCu_2I_3$, PEDOT:PSS, $WO_3$, CuI, and ZnO.[15–23] Li's research confirmed that a heterostructure PD possesses a certain improvement in light response compared with a single-material PD.[24] The rise and decay times of $Ga_2O_3$/CuSCN heterojunction photodetectors are 0.19 s and 0.16 s, faster than those of independent CuSCN and $Ga_2O_3$ devices, indicating that the constructed n-$Ga_2O_3$/p-CuSCN heterojunction can effectively improve the photoresponse speed. Yan[25,26] constructed an organic–inorganic hybrid junction n-$\beta$-$Ga_2O_3$/p-spiro-MeOTAD PD. The influence of spiro thickness on the photoelectric performance of devices

†Corresponding author. E-mail: whtang@njupt.edu.cn

© 2023 Chinese Physical Society and IOP Publishing Ltd 

was investigated in detail. The optimal device was achieved, with an ultrahigh responsivity of 192 mA/W under 254 nm light with a weak illumination of 2 μW/cm$^2$ at zero bias. Currently, a $Ga_2O_3/V_2O_5$ heterostructure PD was designed to produce a superhigh solar-blind spectral discriminability with a deep ultraviolet/visible rejection ratio of $6.0 \times 10^4$, a photo-to-dark current ratio (PDCR) of $2.6 \times 10^7$, an on/off switching ratio of $1.87 \times 10^5$ and a high responsivity of 19.8 mA/W in self-powered mode (0 V).[27]

$Bi_2WO_6$ is an environmentally friendly n-type semiconductor material with many inherent and research-worthy properties, such as piezoelectric, ferroelectric, pyroelectric and good light-harvesting ability.[28–30] It has a suitable band gap of about 2.8 eV, and can be used to detect UV-visible light. Furthermore, $Bi_2WO_6$ has a perovskite lamella structure formed by alternating layers of $Bi_2O_2^{2+}$ and $WO_4^{2-}$ along the *c*-axis. The unique layered structure of $Bi_2WO_6$ endows it with a great possibility to form a heterojunction with $Ga_2O_3$ films through van der Waals forces. However, $Bi_2WO_6$ is rarely used as a light-transmitting material for solar-blind UV detection.

In this work, a $Ga_2O_3/Bi_2WO_6$ heterojunction was fabricated by spin-coating hydrothermally grown $Bi_2WO_6$ onto MOCVD-grown $Ga_2O_3$ film. Based on the $Ga_2O_3/Bi_2WO_6$ heterojunction, a self-powered solar-blind UV PD with a distinct open-circuit voltage was constructed. The PD exhibits an excellent photodetection performance with an ultra-low dark current, a large light-to-dark current ratio, and a fast transient response under zero voltage at 254 nm UV light. Furthermore, a relative band structure diagram of $Ga_2O_3$ and $Bi_2WO_6$ is provided to illustrate and analyze the inherent physical mechanism of the UV light-driven self-powered heterostructure photodetector.

## 2. Experimental details

### 2.1. Fabrication of $Ga_2O_3/Bi_2WO_6$ heterostructure photodetector

$Ga_2O_3$ thin films were grown on wafer-scale sapphire substrate by MOCVD at 500 °C and 25 Torr (1 Torr = $1.33322 \times 10^2$ Pa) with triethylgallium (TEGa), high-purity oxygen ($O_2$) gas and argon (Ar) gas as the gallium source, oxygen source and carrier gas, respectively. The $Bi_2WO_6$ was synthesized using the hydrothermal method according to reference.[31] The derived $Bi_2WO_6$ powder was cleaned, dried and then dispersed in dimethyl sulfoxide (DMSO, AR, Aladdin) to obtain a stable $Bi_2WO_6$ solution of 1 mg/mL by sonicating for 1 h followed by continuous stirring for 6 h.

The fabrication process of the heterojunction is shown in Fig. 1. First, the wafer-scale $Ga_2O_3$ film was cut into small pieces (10 × 10 mm) and the thermal release tape was half-covered on the surface of one piece of $Ga_2O_3$ film. Then, the previously obtained $Bi_2WO_6$ solution in DMSO was spin-coated on the surface of $Ga_2O_3$ film at a speed of 1500 r/min for 30 s. Afterwards, the integrated $Ga_2O_3/Bi_2WO_6$ heterojunction was formed by annealing and releasing the tape at 120 °C for 10 min on a plate heater. Finally, a pair of metal indium (In) with a diameter of 1 mm and a distance of 1 mm–2 mm were pressed on the surface of the $Ga_2O_3$ and $Bi_2WO_6$ as electrodes to form the $Ga_2O_3/Bi_2WO_6$ heterostructure PD. The In electrode thickness is at least 1000 nm, which is thick enough to block the light spots and avoid the UV light passing through the In electrodes.

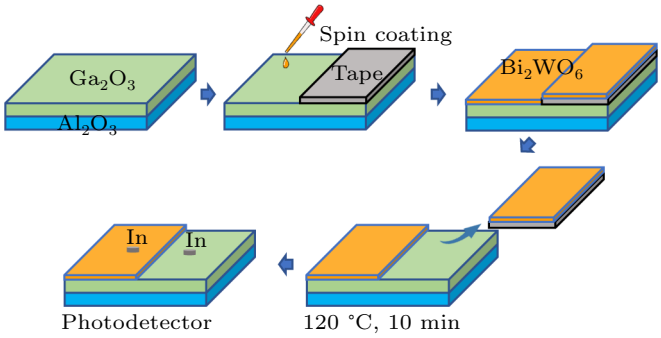



**Fig. 1.** Processes of the fabrication for the $Ga_2O_3/Bi_2WO_6$ heterostructure photodetector.

### 2.2. Characterization and photoresponse measurements

A Bruker AXS D8 Advance x-ray diffractometer (XRD) with a Cu $K\alpha$ radiation source was used to determine the crystalline structure of the $Ga_2O_3/Bi_2WO_6$ heterojunction. Hitachi Regulus 8220 and FEI Verios G4 field-emission scanning electron microscopes (SEM) were utilized to characterize the cross-sectional and surface morphologies of the $Ga_2O_3$ and $Bi_2WO_6$. Low-pressure lamps with wavelengths of 254 nm and 365 nm were used as the ultraviolet (UV) light source. The photoelectric properties of the heterostructure photodetector were measured using a Keysight's B1505A power device analyzer, and the voltages were applied to the $Ga_2O_3$ during the tests.

## 3. Results and discussion

Figure 2(a) shows a high-resolution cross-sectional SEM image of the $Ga_2O_3$ film. It is observed that the $Ga_2O_3$ film grown by MOCVD is very uniform with a thickness of about 310 nm. As shown in Fig. 2(b), the spin-coated $Bi_2WO_6$ on the surface of $Ga_2O_3$ exhibits cluster-like morphologies assembled from sheet-like structures. The XRD pattern of the $Ga_2O_3$ film grown by MOCVD is shown in Fig. 2(c). In addition to the sharp diffraction peaks from the sapphire substrate, there are three obvious diffraction peaks located at 19.11°, 38.83°, and 59.83°, which can be assigned to the $(\bar{2}01)$, $(\bar{4}02)$, and $(\bar{6}03)$ crystal planes of the monoclinic crystal structure of the $\beta$-$Ga_2O_3$ film. Figure 2(d) shows the XRD pattern of the

$Ga_2O_3/Bi_2WO_6$ heterojunction after spin-coating. By careful comparison, three relatively weak extraneous diffraction peaks appear and can be ascribed to the (020), (131), (060), (200), and (002) crystal faces of the orthorhombic $Bi_2WO_6$ (JCPDS No. 39-0256), which suggests successful preparation of the $Ga_2O_3/Bi_2WO_6$ heterojunction.

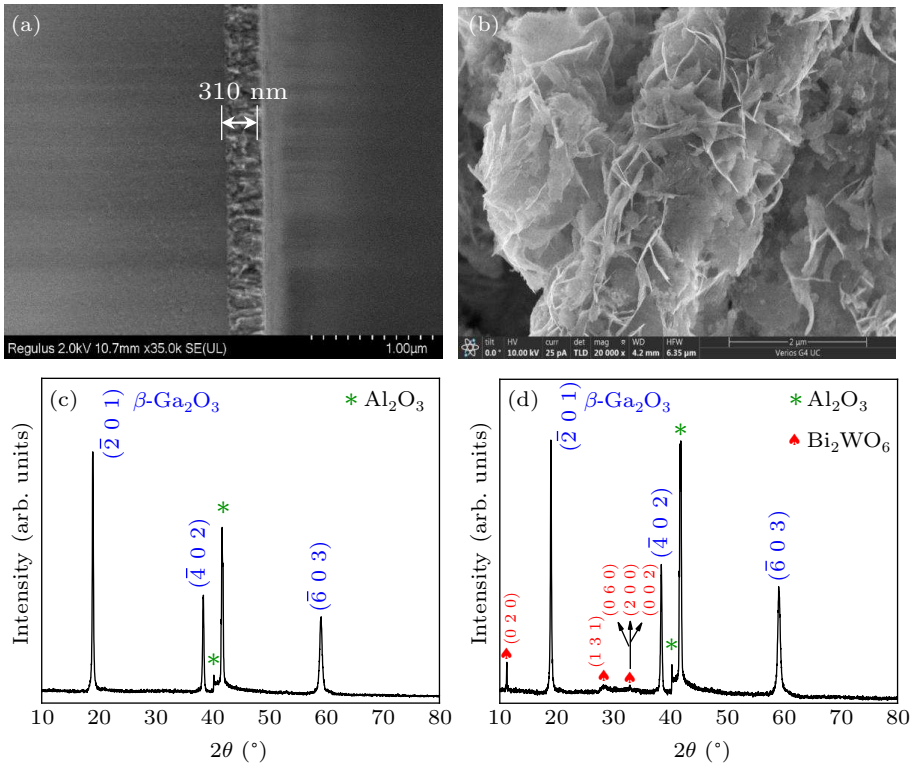



**Fig. 2.** (a) A cross-sectional SEM image of the $Ga_2O_3$ film; (b) an SEM image of $Bi_2WO_6$ surface morphology; XRD patterns of (c) the $Ga_2O_3$ film and (d) the $Ga_2O_3/Bi_2WO_6$ heterojunction.

Figure 3(a) exhibits the *I*–*V* curves of the $Ga_2O_3/Bi_2WO_6$ heterojunction under illumination of the UV light at 254 nm with different light intensities. Under the same voltage, a greater photocurrent ($I_{photo}$) is generated when the PD is radiated by stronger light intensity. This is because a greater number of photo-generated carriers will be excited by the higher light intensity. Similarly, when a larger voltage is applied under the constant incident light intensity, the photo-generated carriers will be separated more efficiently, and thus a larger photocurrent will also be formed. It is noteworthy that the PD exhibits ultra-low dark currents of only $\sim 6$ fA at 0 V and $\sim 55$ fA at 5 V (Fig. 3(b)), which are significantly lower than those of many other reported $Ga_2O_3$-based heterojunctions.[32–34] The extremely low dark currents ($I_{dark}$) can be attributed to a relatively low concentration of defects in the high crystalline quality $\beta$-$Ga_2O_3$ film, as well as an interfacial barrier induced by the formation of a space charge region with the separation of electron–hole pairs at the heterogeneous interface between $Bi_2WO_6$ and $\beta$-$Ga_2O_3$, which can constrain and suppress the carriers across the heterogeneous interface of the heterojunction. Due to the high resistance ($\sim$ T$\Omega$) of the fabricated $Ga_2O_3/Bi_2WO_6$ heterojunction, it does not display notable rectifying behavior.[35] The $I_{photo}$ under 254 nm (331 μW/cm$^2$) UV light are, respectively, 0.2 nA at 0 V and 5.6 nA at 5 V, implying a large PDCR of $3.5 \times 10^4$ at 0 V and $1.0 \times 10^5$ at 5 V (Figs. 3(c) and 3(d)). Additionally, it can be seen in Fig. 3(e) that the constructed $Ga_2O_3/Bi_2WO_6$ exhibits a distinct open-circuit voltage ($V_{OC}$) of $\sim 0.18$ V, as well as the typical photovoltaic effect and self-powered operation behavior. Since the Ohmic contacts have been confirmed via the linear *I*–*V* relationships of the In/$Ga_2O_3$/In and In/$Bi_2WO_6$/In structures in Fig. 3(f), the self-powered behavior is considered to stem from the successful fabrication of the $Ga_2O_3/Bi_2WO_6$ heterojunction. Apart from the significant photocurrent observed at 254 nm, there is a relatively small photocurrent of 0.97 pA at 5 V under the irradiation of 365 nm UV light in Fig. 3(c), which should come from the $Bi_2WO_6$ film in the heterojunction. It is noteworthy that there is a pronounced zero-drift ($\sim 1.8$ V) for the $Bi_2WO_6/Ga_2O_3$ PD under 365 nm light. This can be attributed to the mobile ion-drift induced current[36–38] originating from the intrinsic ionic defects of $Ga_2O_3$ and $Bi_2WO_6$,[39,40] which should be caused by the oxygen ions' migration due to their low activation energy (0.52 eV–0.68 eV).[41] Many interface states will also generate during the formation of the heterojunction between $Bi_2WO_6$ and $Ga_2O_3$. These ionic defects and interface states will trap electrons and lead to dark current hysteresis.[42,43] When illuminated by light, the mobile ion-drift induced current will

be obscured by photogenerated carriers. Because the photo-induced carriers generated under 365 nm UV light are a little too weak to thoroughly overlap with the mobile ion-drift induced current, the pronounced zero-drift (∼ 1.8 V) can still arise under 365 nm light. Once the $Bi_2WO_6/Ga_2O_3$ PD is illuminated with 254 nm light, a large number of photo-induced carriers are generated, which form a considerable photocurrent to overwhelm the mobile ion-drift induced current in the heterojunction. Thus, the mobile ion-drift induced current disappears under 254 nm UV light, and the zero-drift (∼ 0.18 V) in Fig. 3(e) is derived from the depletion layer in the heterojunction with evidence of the self-supply phenomenon at 0 V.

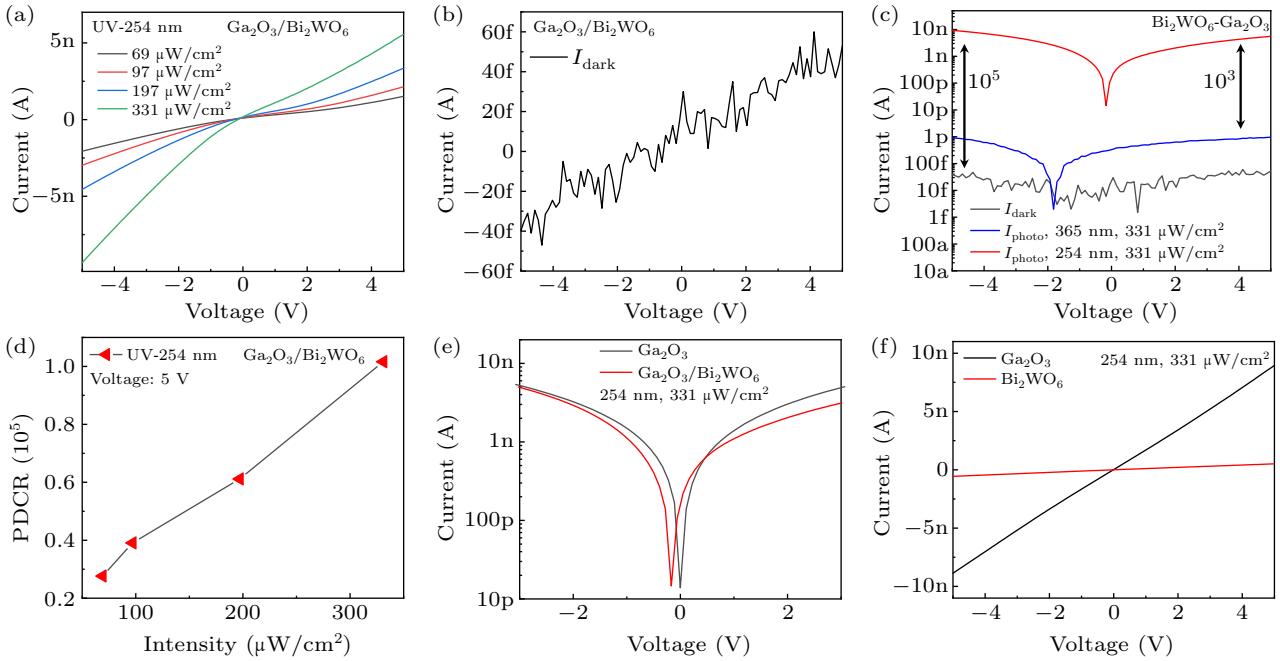



**Fig. 3.** The *I*–*V* curves of the $Ga_2O_3/Bi_2WO_6$ heterojunction (a) under illumination of different light intensities and (b) in dark conditions; (c) *I*–*V* characteristics in a logarithmic coordinate of the $Ga_2O_3/Bi_2WO_6$ PD under dark and illumination conditions; (d) the PDCR of the $Ga_2O_3/Bi_2WO_6$ PD under 254 nm at 5 V voltage; (e) *I*–*V* curves of the $Ga_2O_3$ film and $Ga_2O_3/Bi_2WO_6$ heterojunction under 254 nm UV light; (f) *I*–*V* characteristics of In/$Ga_2O_3$/In and In/$Bi_2WO_6$/In under 254 nm light illumination.

The time-dependent photoresponse performance of the PD under illumination is demonstrated by periodically switching the 254 nm UV lamp on/off every 5 s. As shown in Figs. 4(a) and 4(b), whether being radiated under different light intensities of 69 μW/cm$^2$–331 μW/cm$^2$ or operating at various voltages of 0 V–5 V, the regular step-type *I*–*t* curves indicate that the $Ga_2O_3/Bi_2WO_6$ heterojunction PD can respond quickly and work stably. When the UV lamp is turned on, the photocurrent appears quickly, as a large number of photogenerated carriers are excited by UV light in the heterojunction. When the UV lamp is turned off, the photocurrent disappears rapidly. The self-powered performance test of the PD is displayed in Fig. 4(a). Even though the applied voltage is absent, the PD can still exhibit a good photoresponse to 254 nm UV light. This is because the electron–hole pairs originating from the excitation of UV light can be rapidly separated by the built-in electric field at the interface of the $Ga_2O_3/Bi_2WO_6$ heterojunction. Moreover, the photocurrent exhibits a nonlinear relationship with light intensity, and a power-law function, $I_{photo} \propto P^{\theta}$, can be used to further investigate the numerical relation of the photocurrent with the light intensities ($P$), where $\theta$ is an index reflecting the degree of photoresponse. The fitted curve is plotted in Fig. 4(c); the $\theta$ is estimated to be 0.358 and suggests a high number of intrinsic defects inside the heterojunction, which may be caused by the numerous layers and interfaces between the clustered $Bi_2WO_6$ and $Ga_2O_3$ films after spin coating. Responsivity ($R$) is a key parameter that assesses the photoelectric conversion performance of a PD to a certain light signal.[26] As shown in Fig. 4(d), the responsivity decreases from 2.21 mA/W to 1.68 mA/W as the light intensity increases from 97 μW/cm$^2$ to 331 μW/cm$^2$. This is because the self-heating phenomenon will be induced, and the charge carriers will be more prone to scattering and recombination when the UV light intensity is stronger than 97 μW/cm$^2$, although more electron–hole pairs will generate.

The transient response of the $Ga_2O_3/Bi_2WO_6$ heterojunction was further investigated. The *I*–*t* curves of the current rise and decay processes of the PD are fitted by the following second-order exponential equation: $I = I + A\,e^{t/\tau_r} + B\,e^{-t/\tau_d}$, where $I$ is the steady-state photocurrent, $A$ and $B$ are constants, $t$ is time, and $\tau$ is the relaxation time constant.[19] The fitted rise time ($\tau_r$) and decay time ($\tau_d$) of the ultraviolet transient response curves under different voltages (0 V, 1 V, and 5 V) are shown in Fig. 5. It is noteworthy that the transient response curves show different uptrends under different voltages at 254 nm UV light. At zero voltage, the PD exhibits a fast rise

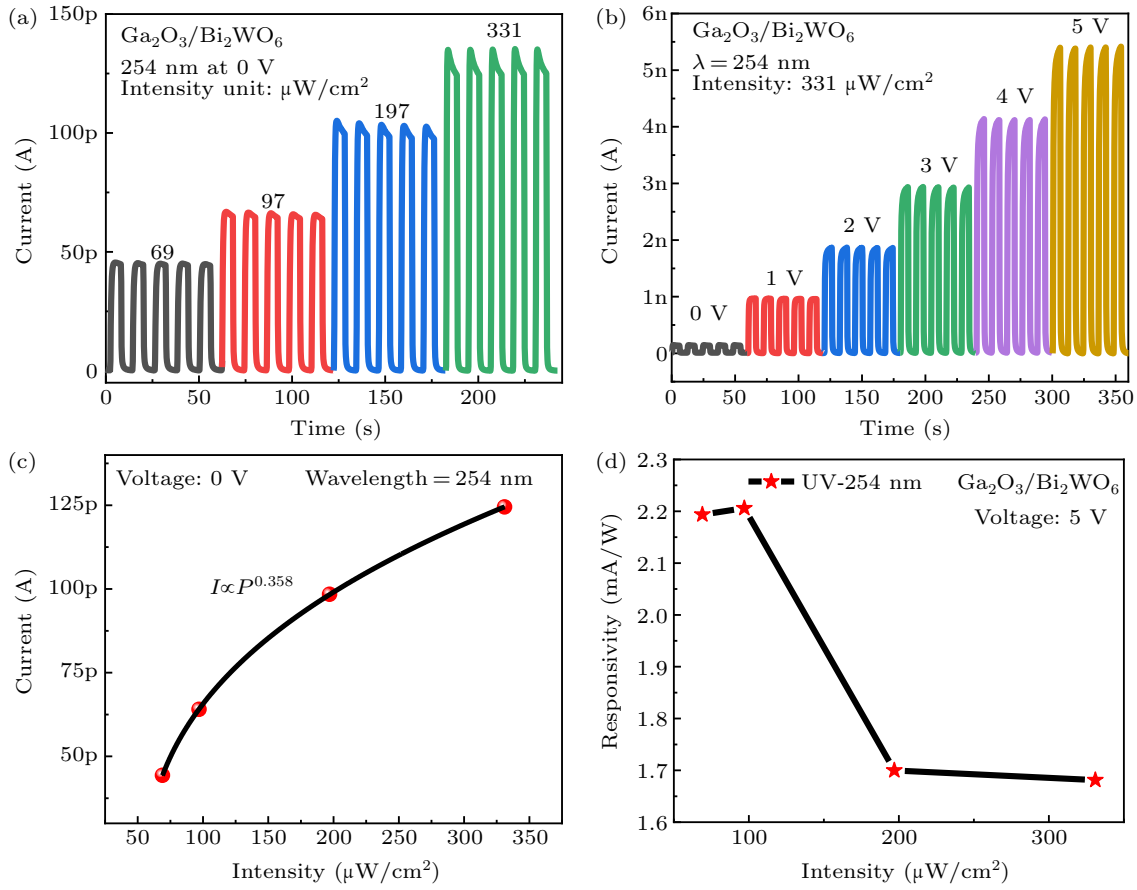



**Fig. 4.** The time-dependent photoresponse of the $Ga_2O_3/Bi_2WO_6$ PD (a) at 0 V with various 254 nm light intensities; (b) under 254 nm UV light with 331 μW/cm² illumination at various voltages; (c) the fitted nonlinear relation curve of the photocurrent with the light intensities; (d) the responsivity with an intensity from 69 mW/cm² to 331 mW/cm² at 5 V voltage.

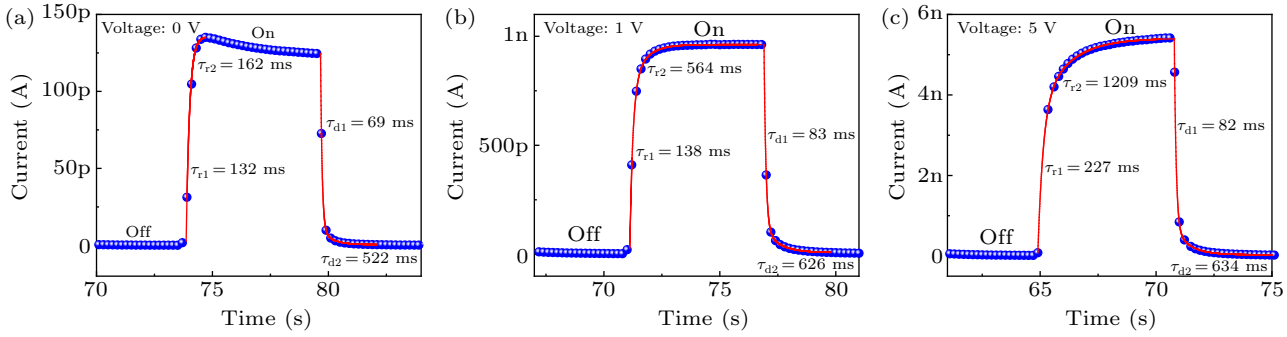



**Fig. 5.** The fitted transient photocurrent response curve under 254 nm UV light at (a) 0 V, (b) 1 V, and (c) 5 V.

time, $\tau_{r1}$ and $\tau_{r2}$ (132 ms and 162 ms), as well as a quick decay time, $\tau_{d1}$ and $\tau_{d2}$ (69 ms and 522 ms), respectively. Obviously, there is a significant photocurrent overshoot phenomenon at zero voltage (Fig. 5(a)). This is mainly due to the fact that a large number of photogenerated electrons and holes generate when the PD is illuminated by the strong 254 nm UV light. The photo-generated carriers cannot be transported to the external circuit promptly due to the non-radiative recombination and the relatively small built-in electric field in the heterojunction at zero voltage, thus resulting in instantaneous charge aggregation and crowding. Certainly, the overshooting phenomenon disappears when a voltage is applied, which can contribute to the separation of charge carriers and suppression of non-radiative recombination. It can be found that as the voltage increases from 1 V to 5 V, the rise time increases while the decay time slightly reduces at 254 nm UV light (Figs. 5(b) and 5(c)). The persistent photoconductivity[44] can be used to explain this rise time dependence with increasing voltage. A higher applied electric field induced by a higher voltage will facilitate the release of photogenerated electrons and holes from defect centers; the photoconductive gain becomes larger but at the expense of a slower photo response speed.[21] This could be due to the limited electron collection capacity of the electrode pairs or the existence of defects at the heterojunction interface; the electrons become relatively congested when passing through these interfaces at a higher voltage, resulting

in a slower response speed of the device. The delay time is mainly determined by the recombination process,[45] and the similar delay times under 1 V and 5 V indicate the relatively stable trapping states.

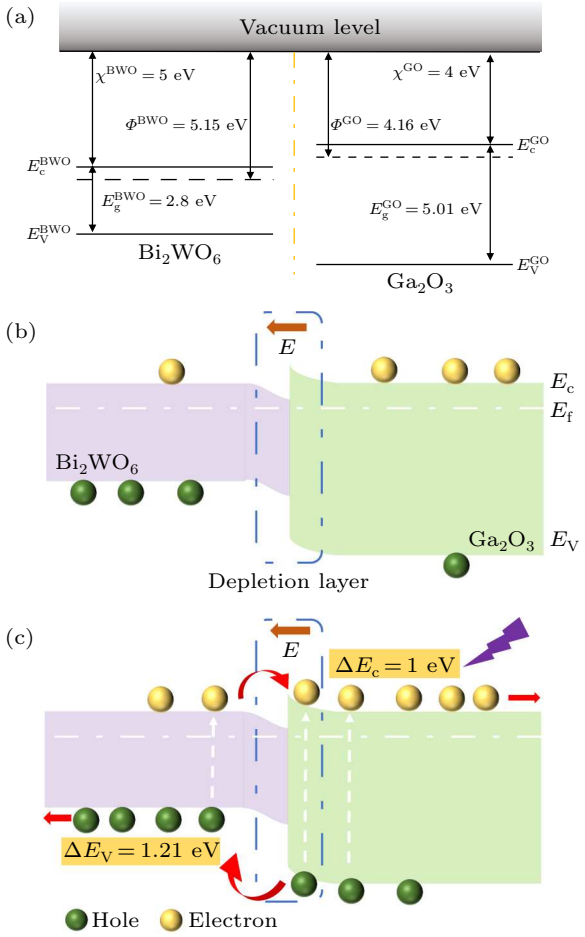



**Fig. 6.** Schematic energy band diagrams of the (a) $Ga_2O_3$ and $Bi_2WO_6$, and the constructed heterojunction under (b) dark and (c) ultraviolet illumination at zero voltage.

Figure 6(a) presents a relative band structure diagram of $Ga_2O_3$ and $Bi_2WO_6$ to illustrate the inherent physical mechanism of self-powered photodetection based on the constructed heterojunction. The electron affinity ($\chi$), work function ($\Phi$) and band gap ($E_g$) of $\beta$-$Ga_2O_3$ and $Bi_2WO_6$ are determined as 4.0 eV, 4.16 eV, and 5.01 eV, and 5.0 eV, 5.15 eV, and 2.8 eV, respectively.[46] As shown in Fig. 6(b), a typical I-type band alignment with an electronic barrier is formed at the interface of the $Ga_2O_3/Bi_2WO_6$ n–n heterojunction. According to Anderson's electron affinities rule,[47] the vacuum electron level is always continuous when $Bi_2WO_6$ and $Ga_2O_3$ form a heterojunction. Once the two come into contact, electrons will transfer from $Ga_2O_3$ to $Bi_2WO_6$ while holes will diffuse in the opposite direction, as the Fermi level position of $Ga_2O_3$ is higher than that of $Bi_2WO_6$. $Ga_2O_3$ forms a positive space charge region (electron depletion region) close to the interface, while $Bi_2WO_6$ forms a negative space charge region (hole depletion region) near the interface. The energy levels of $Bi_2WO_6$ and $Ga_2O_3$ near the interface will bend upward and downward until the Fermi levels are aligned, respectively. A stable built-in electric field will form at the interface from $Ga_2O_3$ to $Bi_2WO_6$. When UV light is illuminated, considerable ground-state electrons will be excited from the valence band to the conduction band, and these photo-generated electrons and holes will overcome the potential barrier and promptly transport away to form a photocurrent on the external circuit under the drive of the built-in electric field (Fig. 6(c)). Therefore, a UV light-driven self-powered mode is realized in this $Ga_2O_3/Bi_2WO_6$ heterojunction photodetector.

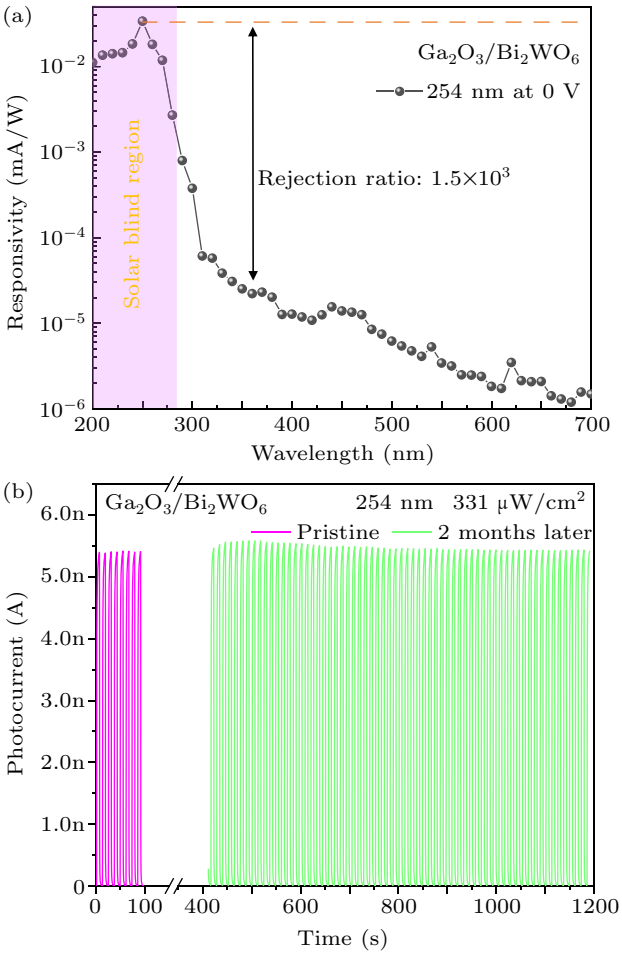



**Fig. 7.** (a) The spectral response of the $Ga_2O_3/Bi_2WO_6$ heterojunction PD at 0 V; (b) the reliability of the $Ga_2O_3/Bi_2WO_6$ heterojunction PD measured after being stored in the atmosphere for two months.

Figure 7(a) illustrates the spectral responsivity of the $Ga_2O_3/Bi_2WO_6$ heterojunction PD at 0 V with the wavelength ranging from 200 nm to 700 nm. The rapid reduction from 260 nm to 300 nm in the responsivity–wavelength curve indicates that our $Ga_2O_3/Bi_2WO_6$ heterojunction PD works in the solar-blind spectral region. Furthermore, the constructed $Ga_2O_3/Bi_2WO_6$PD possesses a great spectrum selectivity with an $R_{250\ nm}/R_{360\ nm}$ rejection ratio of $1.5 \times 10^3$. To validate the operational reliability of the $Ga_2O_3/Bi_2WO_6$ PD, the transient response of the $Ga_2O_3/Bi_2WO_6$ PD after storage in the atmosphere for two months was measured. As shown in

Fig. 7(b), the PD can still demonstrate a timely and sensitive photoresponse to 254 nm UV light (331 μW/cm$^2$) and keeps the unattenuated photocurrent two months later. After operating continuously for 770 s with 77 periodic on/off switching, the transient response also maintains great repeatability, as before. The stable photocurrent and the reproducible operation states demonstrate the great stability of the fabricated $Ga_2O_3/Bi_2WO_6$ PD. In summary, the self-powered UV photodetector based on the $Ga_2O_3/Bi_2WO_6$ heterojunction performs well with an ultra-low noise and a stable photoresponse. A comprehensive performance comparison between our $Ga_2O_3/Bi_2WO_6$ heterojunction PD and other recently reported $Ga_2O_3$-based heterojunction PDs is summarized in Table 1.

**Table 1.** Photodetector performance comparisons with other recently reported $Ga_2O_3$-based heterojunction PDs.

| Heterojunction | UV light (nm) | Self-power | $I_{dark}$ (A) | PDCR | $\tau_r$ (ms)/$\tau_d$ (ms) | Ref. |
|---|---|---|---|---|---|---|
| | | | $6.3\times10^{-15}$@0 V | $3.5\times10^{4}$@0 V | | |
| $Ga_2O_3/Bi_2WO_6$ | 254 | Yes | $5.5\times10^{-14}$@5 V | $1.0\times10^{5}$@5 V | 132/69 | this work |
| | | | $4.2\times10^{-14}$@−5 V | $2.2\times10^{5}$@−5 V | | |
| p-CuSCN/n-$Ga_2O_3$ | 254 | Yes | $1.4\times10^{-11}$@−5 V | $1.29\times10^{4}$@−5 V | 450/260 | [24] |
| $Cs_3Cu_2I_5/\beta$-$Ga_2O_3$ | 265 | Yes | $1.2\times10^{-12}$@0 V | $5.1\times10^{4}$@0 V | $37^{\Delta}/45^{\Delta}$ | [32] |
| $\beta$-$Ga_2O_3$/4H-SiC | 254 | No | $1.67\times10^{-10}$@−10 V | $3.84\times10^{2}$@−10 V | $180^{\Delta}/310^{\Delta}$ | [48] |
| Diamond/$\beta$-$Ga_2O_3$ nano-layer | 254 | No | $<1.0\times10^{-12}$@−15 V | $3.9\times10^{3}$@−15 V | $560^{\Delta}/95^{\Delta}$ | [49] |
| $Ga_2O_3$/NiO | 245 | Yes | $1.09\times10^{-9}$@−15 V | $9.15\times10^{3}$@−15 V | 12/8 | [50] |
| $\beta$-$Ga_2O_3/\gamma$-CuI | 254 | Yes | $4.7\times10^{-13}$@−5 V | $1.08\times10^{5}$@−5 V | 28/199 | [20] |
| $CH_3NH_3PbI_3/\beta$-$Ga_2O_3$ | 254 | No | $5.6\times10^{-10}$@10 V | $1.46\times10^{3}$@10 V | $110/450^{\Delta}$ | [36] |
| $\beta$-$Ga_2O_3/\alpha$-$MoO_3$ | 254 | Yes | $2.31\times10^{-12}$@10 V | $3\times10^{3}$@10 V | 430/640 | [35] |
| PEDOT:PSS/$\beta$-$Ga_2O_3$ | 255 | Yes | $8.46\times10^{-9}$@0 V | – | $60^{\Delta}/88^{\Delta}$ | [51] |
| $MoS_2/\beta$-$Ga_2O_3$ | 245 | Yes | $9\times10^{-13}$@0 V | $\sim6.7\times10^{2}$@0 V | – | [52] |
| Graphene/$\beta$-$Ga_2O_3$ | 254 | – | $1.1\times10^{-6}$@2 V | – | $84830^{\Delta}/219190^{\Delta}$ | [53] |

Note: marked by Δ means that the rise time was obtained from 10% to 90% of the peak output photocurrent; correspondingly, the decay time was obtained from 90% to 10% of the peak output photocurrent.

## 4. Conclusion

In summary, a self-powered solar-blind UV PD was constructed on a $Ga_2O_3/Bi_2WO_6$ heterojunction, which was fabricated by spin-coating hydrothermally grown $Bi_2WO_6$ onto MOCVD-grown $Ga_2O_3$ film. A typical type-I heterojunction is formed at the interface of the $Ga_2O_3$ film and clustered $Bi_2WO_6$. A distinct photovoltaic effect with an open-circuit voltage of 0.18 V is demonstrated under the irradiation of 254 nm UV light. Moreover, the $Ga_2O_3/Bi_2WO_6$ PD displays an excellent photodetection performance with an ultra-low dark current of $\sim$ 6 fA, a high PDCR of $3.5\times10^4$, a fast rise time of 132 ms and 162 ms, as well as a quick decay time of 69 ms and 522 ms in self-powered mode (0 V). Furthermore, a best responsivity result of 2.21 mA/W is also received in power supply mode (5 V). The newly attempted $Ga_2O_3/Bi_2WO_6$ heterojunction provides an important opportunity for the broadening of heterojunction materials and further investigations on $Ga_2O_3$-based self-power solar-blind photodetectors in the future.

## Acknowledgments

Project supported by the National Key Research and Development Program of China (Grant No. 2022YFB3605404), Natural Science Research Start up Foundation of Recruiting Talents of Nanjing University of Posts and Telecommunications (Grant Nos. XK1060921119, XK1060921115, and XK1060921002), National Natural Science Foundation of China (Grant No. 62204125), and China Postdoctoral Science Foundation (Grant No. 2022M721689).

## References

[1] Liu Z, Wang X, Liu Y Y, Guo D Y, Li S, Yan Z Y, Tan C K, Li W J, Li P G and Tang W H 2019 *J. Mater. Chem. C* **7** 13920
[2] Kaur D and Kumar M 2021 *Adv. Opt. Mater.* **9** 2002160
[3] Razeghi M 2002 *Proc. IEEE* **90** 1006
[4] Takeuchi I, Yang W, Chang K S, Aronova M A, Venkatesan T, Vispute R D and Bendersky L A 2003 *J. Appl. Phys.* **94** 7336
[5] Zhou H T, Cong L J, Ma J G, Chen M Z, Song D Y, Wang H B, Li P, Li B S, Xu H Y and Liu Y C 2020 *J. Alloys Compd.* **847** 156536
[6] Hou X H, Zhao X L, Zhang Y, Zhang Z F, Liu Y, Qin Y, Tan P J, Chen C, Yu S J and Ding M F 2022 *Adv. Mater.* **34** 2106923
[7] Han Z Y, Liang H L, Huo W X, Zhu X S, Du X L and Mei Z X 2020 *Adv. Opt. Mater.* **8** 1901833
[8] Roy R, Hill V G and Osborn E F 1952 *J. Am. Chem. Soc.* **74** 719
[9] Liu Z, Zhi Y S, Zhang M L, Yang L L, Li S, Yan Z Y, Zhang S H, Guo D Y, Li P G and Guo Y F 2022 *Chin. Phys. B* **31** 088503
[10] Liu Z, Li P G, Zhi Y S, Wang X L, Chu X L and Tang W H 2019 *Chin. Phys. B* **28** 017105
[11] Qin Y, Long S B, Dong H, He Q M, Jian G Z, Zhang Y, Hou X H, Tan P J, Zhang Z F and Lv H B 2019 *Chin. Phys. B* **28** 018501
[12] Zhang M L, Liu Z, Yang L L, Yao J F, Chen J, Zhang J, Wei W, Guo Y F and Tang W H 2022 *Crystals* **12** 406
[13] Mastro M A, Kuramata A, Calkins J, Kim J, Ren F and Pearton S J 2017 *ECS J. Solid State Sci. Technol.* **6** P356
[14] Oshima Y, Vllora E G and Shimamura K 2015 *J. Cryst. Growth* **410** 53
[15] Gao A, Jiang W Y, Ma G L, Liu Z, Li S, Yan Z Y, Sun W M, Zhang S H and Tang W H 2022 *Curr. Appl. Phys.* **33** 20
[16] Li S, Yan Z Y, Liu Z, Chen J, Zhi Y S, Guo D Y, Li P G, Wu Z P and Tang W H 2020 *J. Mater. Chem. C* **8** 1292
[17] Li S, Yue J Y, Wu C, Liu Z, Yan Z Y, Li P G, Guo D Y, Wu Z P, Guo Y F and Tang W H 2021 *IEEE Sens. J.* **21** 26724

[18] Li S, Zhi Y S, Lu C, Wu C, Yan Z Y, Liu Z, Yang J, Chu X L, Guo D Y and Li P G 2021 *J. Phys. Chem. Lett.* **12** 447

[19] Ma G L, Jiang W Y, Sun W M, Yan Z Y, Sun B Y, Li S, Zhang M L, Wang X, Gao A and Dai J 2021 *Phys. Scr.* **96** 125823

[20] Sun W M, Sun B Y, Li S, Ma G L, Gao A, Jiang W Y, Zhang M L, Li P G, Liu Z and Tang W H 2021 *Chin. Phys. B* **31** 024205

[21] Yan Z Y, Li S, Liu Z, Liu W J, Qiao F, Li P G, Tang X, Li X H, Yue J Y and Guo Y F 2022 *IEEE J. Sel. Top. Quantum Electron.* **28** 3803208

[22] Zhao B, Wang F, Chen H Y, Zheng L X, Su L X, Zhao D X and Fang X S 2017 *Adv. Funct. Mater.* **27** 1700264

[23] Liu Z, Liu Y Y, Wang X, Li W J, Zhi Y S, Wang X L, Li P G and Tang W H 2019 *J. Appl. Phys.* **126** 045707

[24] Sun B Y, Sun W M, Li S, Ma G L, Jiang W Y, Yan Z Y, Wang X, An Y H, Li P G and Liu Z 2022 *Opt. Commun.* **504** 127483

[25] Yan Z Y, Li S, Yue J Y, Ji X Q, Liu Z, Yang Y T, Li P G, Wu Z P, Guo Y F and Tang W H 2021 *J. Mater. Chem. C* **9** 14788

[26] Yan Z Y, Li S, Yue J Y, Liu Z, Ji X Q, Yang Y T, Li P G, Wu Z P, Guo Y F and Tang W H 2021 *ACS Appl. Mater. Interfaces* **13** 57619

[27] Li S, Yan Z Y, Tang J C, Yue J Y, Liu Z, Li P G, Guo Y F and Tang W H 2022 *IEEE Trans. Electron Devices* **69** 2443

[28] Zhang X L, Wang H W, Zhang J, Li J X, Ma Z Y, Li J, Leng B, Niu P J and Liu B D 2020 *Nano Energy* **77** 105119

[29] Chen M X, Zhao B, Hu G F, Fang X S, Wang H, Wang L, Luo J, Han X, Wang X D and Pan C F 2018 *Adv. Funct. Mater.* **28** 1706379

[30] Nie J H, Zhang Y, Li L J and Wang J Z 2020 *J. Mater. Chem. C* **8** 2709

[31] Xu X, Ming F W, Hong J Q and Wang Z C 2018 *ACS Mater. Lett.* **9** 188

[32] Ma J L, Xia X C, Yan S, Li Y, Liang W Q, Yan J J, Chen X, Wu D, Li X J and Shi Z F 2021 *ACS Appl. Mater. Interfaces* **13** 15409

[33] Li S, Guo D Y, Li P G, Wang X, Wang Y H, Yan Z Y, Liu Z, Zhi Y S, Huang Y Q and Wu Z P 2019 *ACS Appl. Mater. Interfaces* **11** 35105

[34] Li P G, Shi H Z, Chen K, Guo D Y, Cui W, Zhi Y S, Wang S L, Wu Z P, Chen Z W and Tang W H 2017 *J. Mater. Chem. C* **5** 10562

[35] Cui Y H, Zhang S H, Shi Q S, Hao S C, Bian A, Xie X B and Liu Z 2021 *Phys. Scr.* **96** 125844

[36] Dong L P, Pang T Q, Yu J G, Wang Y C, Zhu W G, Zheng H D, Yu J H, Jia R X and Chen Z 2019 *J. Mater. Chem. C* **7** 14205

[37] Pang T Q, Jia R X, Wang Y C, Sun K, Hu Z Y, Zhu Y J, Luan S Z and Zhang Y M 2018 *Materials* **11** 1606

[38] Zhu X J, Lee J H and Lu W D 2017 *Adv. Mater.* **29** 1700527

[39] Islam M S, Lazure S, Vannier R N, Nowogrocki G and Mairesse G 1998 *J. Mater. Chem.* **8** 655

[40] Šlkus T, Štas L, Kežonis A, Kodols M, Grabis J, Vikhrenko V, Gunes V and Barre M 2015 *Solid State Ionics* **271** 73

[41] Yakimov A V, Filatov D O, Gorshkov O N, Antonov D A, Liskin D A, Antonov I N, Belyakov A V, Klyuev A V, Carollo A and Spagnolo B 2019 *Appl. Phys. Lett.* **114** 253506

[42] Hao W B, He Q M, Zhou K, Xu G W, Xiong W H, Zhou X Z, Jian G Z, Chen C, Zhao X L and Long S B 2021 *Appl. Phys. Lett.* **118** 043501

[43] Park Y, Ma J, Yoo G and Heo J 2021 *Nanomaterials* **11** 494

[44] Zhang Y F, Chen X H, Xu Y, Ren F F, Gu S L, Zhang R, Zheng Y D and Ye J D 2019 *Chin. Phys. B* **28** 028501

[45] Chen X H, Xu Y, Zhou D, Yang S, Ren F F, Lu H, Tang K, Gu S L, Zhang R and Zheng Y D 2017 *ACS Appl. Mater. Interfaces* **9** 36997

[46] Wang H L, Li S J, Zhang L S, Chen Z G, Hu J Q, Zou R J, Xu K B, Song G S, Zhao H H and Yang J M 2013 *CrystEngComm* **15** 9011

[47] Klein A 2012 *Thin Solid Films* **520** 3721

[48] Yu J, Nie Z, Dong L, Yuan L, Li D, Huang Y, Zhang L, Zhang Y and Jia R 2019 *J. Alloys Compd.* **798** 458

[49] Kim H, Tarelkin S, Polyakov A, Troschiev S, Nosukhin S, Kuznetsov M and Kim J 2020 *ECS J. Solid State Sci. Technol.* **9** 045004

[50] Yu J G, Yu M, Wang Z, Yuan L, Huang Y, Zhang L C, Zhang Y M and Jia R X 2020 *IEEE Trans. Electron Devices* **67** 3199

[51] Zhang D, Zheng W, Lin R C, Li Y Q and Huang F 2019 *Adv. Funct. Mater.* **29** 1900935

[52] Zhuo R R, Wu D, Wang Y G, Wu E P, Jia C, Shi Z F, Xu T T, Tian Y T and Li X J 2018 *J. Mater. Chem. C* **6** 10982

[53] Kong W Y, Wu G A, Wang K Y, Zhang T F, Zou Y F, Wang D D and Luo L B 2016 *Adv. Mater.* **28** 10725